Erschienen in: Journal of Applied Physics ; 95 (2004), 3. - S. 1556-1561
https://dx.doi.org/10.1063/1.1636252

Observation of transition metals at shunt locations in multicrystalline silicon solar cells

T. Buonassisi,[a] O. F. Vyvenko,[b] A. A. Istratov, and E. R. Weber
Lawrence Berkeley National Laboratory, University of California, MS 62-203, 1 Cyclotron Road, Berkeley, California 94720

G. Hahn and D. Sontag
University of Konstanz, Department of Physics, P.O. Box X916, 78457 Konstanz, Germany

J. P. Rakotoniaina and O. Breitenstein
Max Planck Institute of Microstructure Physics, Weinberg 2, D-06120 Halle, Germany

J. Isenberg and R. Schindler
Fraunhofer Institute for Solar Energy Systems, Heidenhofstrasse 2, D-79110 Freiburg, Germany

(Received 8 April 2003; accepted 30 October 2003)

By employing a combination of analytical tools including lock-in thermography and synchrotron-based x-ray fluorescence microscopy, transition metals have been identified at shunting locations in two types of low-cost multicrystalline silicon (mc-Si) solar cell materials: cast multicrystalline and ribbon growth on substrate (RGS). At a shunting location in the cast mc-Si cell, silver and titanium, both contact strip materials, have been identified at the shunting location, suggesting a process-induced error related to contact metallization. At a shunting location in the RGS cell, a material-specific shunting mechanism is described, involving channels of inverse conductivity type, where copper and iron are found. The possible roles of these metals in this shunting mechanism are discussed. These results illustrate the wide range of physical mechanisms involved with shunting in solar cells. © *2004 American Institute of Physics.*
[DOI: 10.1063/1.1636252]

I. INTRODUCTION

A rising 93% of the solar cells sold annually worldwide are fabricated from crystalline silicon materials.[1] Representing over half of this quantity are cost-competitive multicrystalline silicon (mc-Si) materials that typically make use of faster and relatively dirtier production techniques. Industrial solar cells fabricated from these mc-Si materials are typically only 12%–16% efficient (with an efficiency as high as 19.8% reported for a 1 cm^2 cell area), compared to efficiencies around 15%–17% for industrial solar cells made of high quality single-crystalline Czochralski or float-zone wafers (with the efficiency of 24.7% reported for a 4 cm^2 cell area).[2]

To explain this discrepancy, it must be noted that low-cost mc-Si materials contain much higher amounts of transition metals, oxygen, carbon, and structural defects relative to integrated circuit grade silicon.[3,4] Transition metals, for example, introduce energy levels into the silicon band gap that, depending on their physical proximity to the solar cell pn junction, can degrade solar cell device performance in a variety of ways. Davis *et al.*[5] have introduced various transition metals into Czochralski silicon during growth, measured the effect of contamination level and type on solar cell device performance, and found a significant reduction of minority carrier diffusion length (L_{diff}) within the bulk, which typically limits the current output of the solar cell. For certain metals in high concentrations, however, it was noticed that changes in L_{diff} alone could not account for the measured $I-V$ characteristics of the solar cell, and that junction effects must play a role. It is known from numerous studies of semiconductor devices that metals in high concentrations have substantial impacts on the $I-V$ characteristics and the effective barrier heights of pn junctions.[6–8] It was therefore hypothesized that transition metals may play a role in producing localized regions of lower pn junction barrier height, either by forming point shunts or regions of increased recombination activity. Both of these defects drain power from other regions of the solar cell with better pn junction properties, significantly reducing the current and voltage outputs under operational conditions, and thus the fill factor (FF) of the solar cell device, which is directly related to the efficiency.[9]

Various experimental techniques have been developed to detect these defective regions in the pn junction and to test their electrical properties.[10–12] The concept of a ''shunt'' was originally conceived as a highly localized defect in the pn junction, ohmic in nature. With the development of more sophisticated characterization techniques such as lock-in thermography, it was found that many point shunts do not exhibit a linear (ohmic) $I-V$ characteristic, but in fact exhibit a rectifying (nonlinear) response to applied forward bias voltage.[13] Further studies revealed a variety of mechanisms leading to the formation of regions of locally increased forward current density, including but not limited to regions with strong recombination activity, linear and nonlinear edge shunts, cracks, holes, and scratches.[14] While respecting this

[a]Electronic mail: buonassisi@socrates.berkeley.edu
[b]On leave of absence from the Institute of Physics, St.-Petersburg State University, Russia.

diversity of the physical causes, the term shunt will in this publication refer to any site of an increased local current density under forward bias, which can be detected as a hot spot in a lock-in thermography map.

The direct correlation of transition metals with a variety of shunting mechanisms has not yet been thoroughly investigated. This is because an experimental procedure combining a high sensitivity to transition metals with micron-scale spatial resolution and high-sensitivity shunt imaging had not been developed. In this study, we apply a combination of state-of-the-art analytical techniques: lock-in thermography, laser beam induced current (LBIC) with variable excitation wavelengths, synchrotron-based x-ray beam induced current (XBIC), and x-ray fluorescence microscopy (μ-XRF) to examine shunts in solar cells. We describe observations and discuss the implications of transition metals present at shunting locations in two types of low-cost mc-Si solar cell materials: cast mc-Si (processed into a solar cell at Fraunhofer ISE), and ribbon growth on substrate (RGS),[15] processed into a solar cell at University of Konstanz.

II. EXPERIMENTAL TECHNIQUE AND SAMPLE PREPARATION

A powerful tool for locating shunts is lock-in thermography. The lock-in thermography technique consists of subjecting the solar cell to a sequence of either forward or reverse bias voltage pulses, which in turn stimulates a current to flow with the same frequency as the bias pulses. More current will tend to flow through the regions of shunts, resulting in a local heating of the solar cell at these locations. With the use of an infrared focal plane array camera coupled to the voltage source frequency, one can capture an image of the local periodic temperature variations across the solar cell surface with a sensitivity of 10 μK or better, making this an ideal nondestructive tool to locate local increases in current density in electronic components.[12,16] The lock-in thermography measurements in this work were performed at Fraunhofer ISE (for cast mc-Si) and at MPI Halle (for RGS), using commercially available equipment by Thermosensorik GmbH.[17]

While lock-in thermography is a very useful technique for spatially locating shunts, it gives no direct information about the chemical species present at a shunt location. For this purpose, we have employed the synchrotron-based μ-XRF technique available at Beamline 10.3.1 of the Advanced Light Source (ALS) of the Lawrence Berkeley National Laboratory.[18] The ALS, a third generation synchrotron, offers an extremely bright and stable source of x rays, enabling the use of specialized focusing optics[19] to obtain a spot size on the order of $1-2\ \mu m^2$ with an optimal $\sim 10^{10}$ photons/s and a peak energy of 12.4 keV. The combination of small spot size and large flux allows the μ-XRF technique to detect a single iron precipitate with radius ~ 18 nm, or homogenous iron concentrations of 10^{14} cm^{-2}. More on the sensitivity limits and applications of the μ-XRF technique can be found elsewhere.[20,21]

In order to correlate μ-XRF with lock-in thermography maps with sufficient accuracy, spectrally resolved laser beam induced current (SR–LBIC) (performed at Fraunhofer ISE for cast mc-Si and University of Konstanz for RGS) and XBIC[22] techniques were employed. SR–LBIC and XBIC techniques can be easily compared since they both map, over the surface of the solar cell, the local current collection efficiency upon illumination. This, in the absence of alternative current collection mechanisms, allows one to draw conclusions about the local minority carrier diffusion length. One-to-one correspondence between illumination induced current collection and shunt location is achieved by overlapping SR–LBIC and thermography maps of the entire solar cell, using the edges of the wafer and contact strips as guides. The accuracy of this superposition is limited by the resolution of each technique and is typically $\sim 300\ \mu$m. In the case of XBIC, the minority charge carriers are generated by the same x-rays that fluoresce the sample. Thus, both XBIC and μ-XRF can be performed simultaneously, providing a one-to-one correspondence between recombination activity and elemental composition with micron-scale resolution. In this manner, shunts can be correlated with transition metal concentrations with a precision that is limited by the resolutions of the lock-in thermography and SR–LBIC techniques.

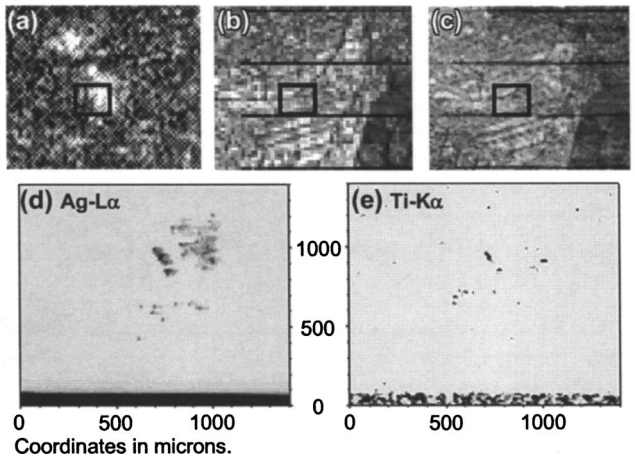

FIG. 1. The process followed to determine the presence of metals at a shunting location in a fully processed cast multicrystalline solar cell: A lock-in thermography map (a) of a 7×9 mm^2 region of the solar cell containing two shunts is correlated with LBIC (b). At the synchrotron, an XBIC map (c) is made over the same region. X-ray fluorescence microscopy [(d) and (e)] is performed on the small subregion containing one shunt [denoted by the box in (a), (b), and (c)]. Silver (d) and titanium (e) appear in quantities comparable to their concentrations in the contact strips (visible at the bottom of the μ-XRF maps). Residues of the contact metallization are likely the cause of this shunt.

III. RESULTS: CAST MATERIAL

A shunt in a fully processed cast multicrystalline silicon solar cell was analyzed using the approach described earlier. Figure 1(a) shows a 7×9 mm^2 region of interest, containing two bright spots, of a lock-in thermography map. These bright spots represent points of increased heat generation, evidence for a locally increased dark forward current flowing through shunts. The shunt featured in Fig. 1(a) was the second-strongest shunt in the solar cell at operating conditions, and unlike the strongest shunt (an edge shunt), this shunt analyzed herein cannot be removed by proper edge isolation. This corresponding region in a SR–LBIC map is

shown in Fig. 1(b). The SR–LBIC and lock-in thermography maps were superimposed using the contact strips as guides, and the position of the shunt located on the SR–LBIC map. At Beamline 10.3.1 of the Advanced Light Source, an XBIC scan was performed [Fig. 1(c)]. Notice the similarity between the XBIC and the SR–LBIC [Fig. 1(b)] maps. This good correlation ensures the coordinates of the shunt can be determined for the purpose of acquiring a detailed μ-XRF map.

Upon a μ-XRF analysis at the shunt location [shown as a small black box in each of Figs. 1(a), 1(b), and 1(c)], high concentrations of silver [Fig. 1(d)] and titanium [Fig. 1(e)] were detected. These metals are used to form the contact fingers of the metallization grid. Despite being found at the shunt location a millimeter away from the nearest contact finger, these metals were present in nearly the same proportions as in the contact strips themselves, which are visible in the lower part of Figs. 1(d) and 1(e). Palladium is also expected to accompany Ag and Ti, since Pd is also a constituent of the contact metallization. However, the Pd–Lα fluorescence peak could not be resolved from the shoulder of the Ag–Lα. The weaker Pd–Lβ_1, Lβ_2, and Lγ peaks overlap with the Ag–Lα_1, Lβ_1, and Lβ_2 peaks, respectively, and are not distinguishable. If Pd is present, we conclude it is certainly at least an order of magnitude less abundant than silver, which again reflects the relative composition of the contact fingers, typically a ratio of Ti:Pd:Ag $=1:1:(300-1000)$.

These facts indicate that this shunt is most likely a process-induced defect that was formed during metallization grid deposition. If silver or palladium is deposited directly on the surface of the wafer without a properly placed titanium buffer layer, then silver and palladium, both relatively fast diffusers in silicon, are likely to diffuse into the space-charge region during the subsequent heat treatment designed to sinter the contact metals. Such a process-induced defect, while not material specific, can be especially deleterious for solar cells with shallow emitters, as was the case with the sample analyzed in this study. It must also be pointed out that similar, albeit more severe, shunting effects have been reported after contact overfiring by Ballif *et al.*[11] and overannealing by Hahn *et al.*[23]

IV. RESULTS: RIBBON GROWTH ON SUBSTRATE MATERIAL

RGS silicon wafer technology is still in the R&D phase at the moment with a full-speed, continuously operating bench-scale machine under development. Two distinguishing features of RGS material are very high oxygen and carbon concentrations (about 2×10^{18} cm^{-3} and 1×10^{18} cm^{-3}, respectively) and the so-called "current collecting channels," which can form during a slow cool at the end of the wafer fabrication process.[24] The existence of channels which collect current from the bulk was first proposed by Häßler *et al.*[25] to explain the extraordinarily large short circuit current (J_{sc}) values of slow-cooled RGS solar cells (>30 mA/cm^2) despite short minority carrier diffusion lengths below 20 μm for as-grown and below 40 μm for hydrogen passivated wafers. This phenomenon was investigated by Breitenstein *et al.*[26] via electron beam induced current (EBIC) measurements performed from the backside of a slow-cooled RGS solar cell along a beveled surface. Surprisingly, it was found that a significant EBIC signal was detected at points corresponding to etch pit defects, even when the electron-hole pair generation volume was tens or hundreds of microns away from the emitter. It was also known from analytical electron microscopy[27] and spatially resolved secondary ion mass spectroscopy studies[24] that extended structural defects in slow-cooled RGS material can be densely covered with oxygen and carbon precipitates. In addition, transmission electron microscopy studies by Werner at MPI Halle[24] showed that extended structural defects from regions of the wafer with abnormally high internal quantum efficiencies (that can only be explained by the presence of current collecting channels) are heavily and continuously decorated with precipitates, whereas extended structural defects from regions of the wafer with standard diffusion lengths are not. With this secondary information, and by observing the coincidence of defect etch pits with increased EBIC signal in the bulk far from the emitter, it was concluded from the study of Breitenstein *et al.*[26] that the physical nature of current collecting channels is oxide and carbide coated extended structural defects, which form a three-dimensional network of inversion channels extending from the emitter into the bulk. Further details can be found elsewhere.[26]

TABLE I. Device parameters for three different 20×20 mm^2 hydrogen passivated RGS solar cells with high, medium, and low densities of current collecting channels.

Amount of current collecting channels	FF	Open circuit voltage (V_{oc}) (mV)	Short circuit current (J_{sc}) (mA/cm^2)	Efficiency
High	56.6%	518.2	21.9	6.42%
Medium	66.9%	543.3	17.0	6.16%
Low	76.6%	548.5	17.2	7.23%

The theoretical benefits of current collecting channels are obvious: an extension of the effective pn junction of the solar cell along channels leading into the bulk should equate into an increased current output of the device, especially for materials with relatively short minority carrier diffusion length. However, as more investigations[24] were made into the effectiveness of current collecting channels for improving device performance, it was found that RGS solar cells with an abundance of these channels tend to have lower open circuit voltages and fill factors than their counterparts with fewer channels, as shown in Table I. Hence, it is clear that current collecting channels in their present form are globally detrimental to cell performance.

The lower FF and V_{oc} for cells with higher amounts of current collecting channels suggest that the pn-junction properties of the space charge region surrounding the current collecting channels are very different from those of the space charge region of the emitter. Specifically, the barrier heights of the pn junctions surrounding at least some of the current collecting channels must be lower than the effective emitter pn-junction barrier height at forward biases, producing

lower V_{oc} and FF values that offset the benefits of increased current collection. In the following subsections we describe the experimental procedures which allowed us to identify current collecting channels in an RGS sample, correlate them with hot spots in a lock-in thermography map, and demonstrate the presence of metal clusters at these channels.

A. XBIC/long-λ LBIC detection of current collecting channels

In this experiment, the 20×20 mm^2 RGS solar cell with medium density of current collecting channels was studied (device parameters appear in Table I). Short ($\lambda = 635$ nm), medium (910 nm), and long (980 nm) wavelength LBIC were performed, as shown in Figs. 2(a), 2(b), and 2(c), respectively. 635 nm light penetrates only 3 μm below the sample surface, while 910 nm light penetrates approximately 37 μm, and 980 nm light penetrates much deeper, to about 104 μm. Although bulk minority carrier diffusion length values are typically below 40 μm for processed RGS material after hydrogen passivation, regions of unexpectedly high current collection efficiencies are nonetheless observed in long-wavelength LBIC, [Fig. 2(b) and especially Figs. 2(c) and 3(b)] and XBIC performed at 12.4 keV [Fig. 3(c)]. This phenomenon can be explained by the presence of current collecting channels at these regions: the minority carriers generated deep within the bulk by the long wavelength light need only diffuse the short distance to the current collecting channel, not all the way to the surface *pn* junction. On the other hand, LBIC performed with short wavelength light [Fig. 2(a)] does not demonstrate an enhanced current collection in these same regions because of the shallow penetration depth of the light; in this case, most photogenerated minority carriers are well within one diffusion length, L_{diff}, from the surface of the wafer and can readily be collected by the emitter *pn* junction. In fact, with short wavelength excitation, regions of current collecting channels actually demonstrate slightly less collected current than regions with only the surface emitter *pn* junction.

B. Lock-in thermography and current collecting channels

Lock-in thermography, which measures the solar cell in nonilluminated forward (or reverse) bias conditions, forces electrons to flow from the emitter into the bulk preferentially through regions of reduced *pn*-junction barrier height, which creates the hot spots observed by the infrared camera. With the wafer surface parallel to the camera lens, any heat produced along a current collecting channel protruding into the bulk—along the third dimension—will be projected onto a spot on the two-dimensional thermography map (taking lateral heat diffusion into consideration). Thus, any homogeneously distributed effect along the length of a current collecting channel will create the effect of a local ''hot spot'' in a lock-in thermography image.

Figure 3 presents a comparison between lock-in thermography (a), long (980 nm) wavelength LBIC (b), and XBIC (c), revealing that regions of increased lock-in thermography signal correspond to regions of increased current collection. High frequency lock-in thermography taken at

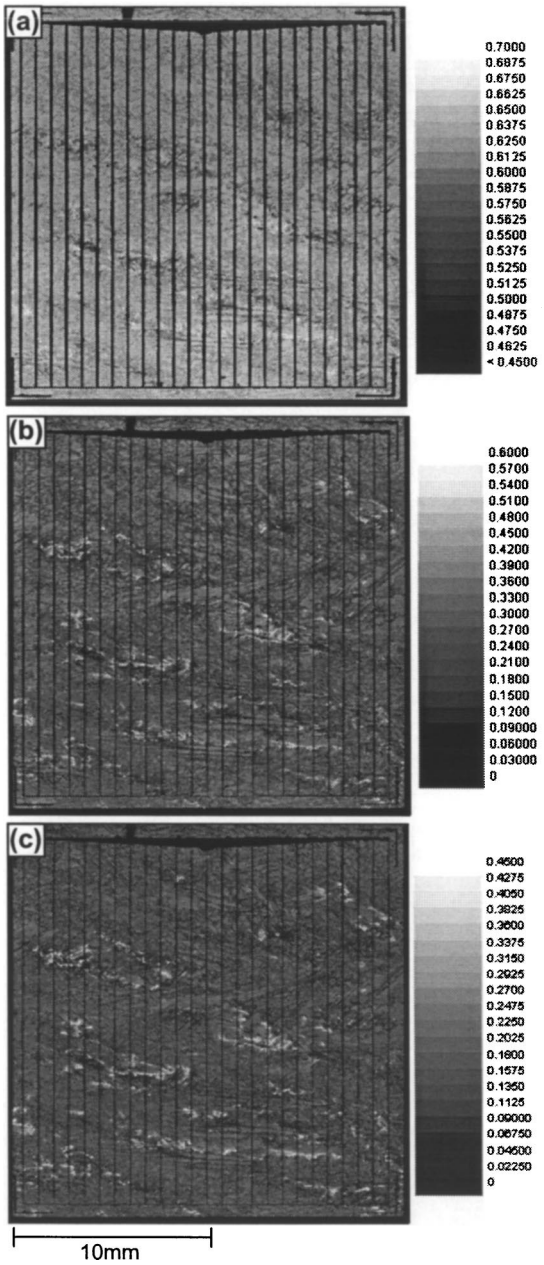

FIG. 2. Comparison of short [(a) $\lambda = 635$ nm, penetration depth ~ 3 μm], medium [(b) $\lambda = 910$ nm, $d_{\text{pen}} \sim 37$ μm] and long [(c) $\lambda = 980$ nm, $d_{\text{pen}} \sim 104$ μm] wavelength LBIC maps of the same 20×20 mm^2 RGS solar cell. As the penetration depth of the excitation light exceeds the minority carrier diffusion length ($L_{\text{diff}} < 40$ μm), current collecting channels become the dominant minority carrier collection mechanism, appearing as bright regions in (b) and (c). These same regions appear darker when probed with shorter wavelengths (a), when most photogenerated carriers are within one minority carrier diffusion length from the surface (emitter) *pn* junction. Units are in external quantum efficiency.

$f_{\text{lock-in}} = 54$ Hz ensures minimum heat diffusion between imaging, and thus a sharp image of the heat source which matches well in shape and size with the features of the current collecting channels revealed by LBIC and XBIC. This result indicates that the increased current flow observed in lock-in thermography originates below the surface of the wafer, at regions with high densities of current collecting channels, and not from a coincidental defect in the emitter *pn* junction near the surface of the wafer.

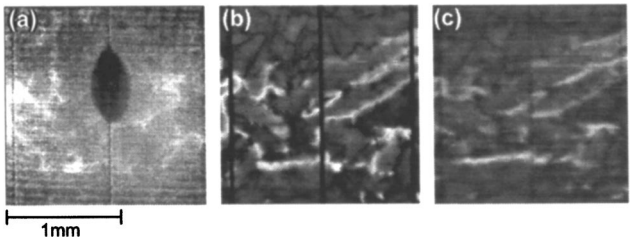

FIG. 3. Detail of a shunt area in an RGS sample. The features evident in the 54 Hz lock-in thermography image taken at 0.52 V forward bias (a) resemble those of the 980 nm LBIC (b) and XBIC (c) maps of this area taken at zero bias, indicating that the shunting current is generated at or near the current collecting channels. The oval marker evident in (a) was placed on the surface of the solar cell to mark the region of interest.

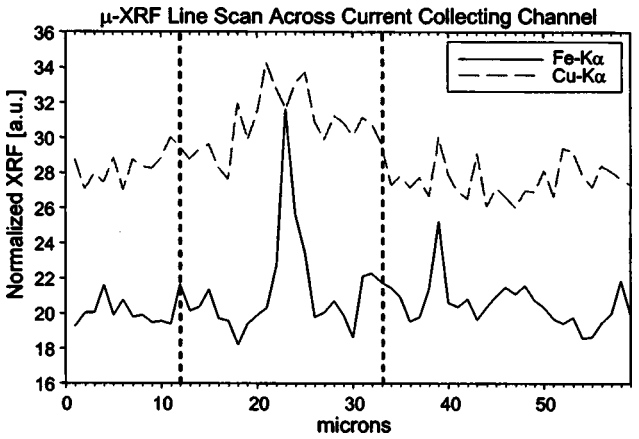

FIG. 4. An x-ray fluorescence microscopy line scan reveals an increase of copper and iron at a current collecting channel (between vertical dashed lines, identified by XBIC). A lower bound for the peak Fe concentration is 1.7×10^{14} cm^{-2} and Cu 1.5×10^{14} cm^{-2}. This result suggests that current collecting channels are effective gettering sites for transition metals, which may play a role in shunt formation.

The electrical properties of the space charge region surrounding a current collecting channel are decidedly different than those of the emitter pn junction. The ideality factor of the dark forward current produced at the current collecting channels, measured by performing lock-in thermography at different bias voltages (more information on extraction of local $I-V$ characteristics can be found elsewhere),[13] was determined to be $n=5$. This ideality factor is very large compared to those of diffused emitter pn junctions, which typically vary between $n=1-2$ and can be well-explained by theory.[28–30] This large ideality factor, which is prominent in the $I-V$ characteristics for solar cells with high densities of current collecting channels, also explains the lower fill factors observed for cells with increasing densities of current collecting channels, as shown in Table I.

C. X-ray fluorescence microscopy and transition metal distributions

The μ-XRF tool at Beamline 10.3.1 of the ALS was employed to determine the presence of transition metals at the current collecting channels. First, the location of a current collecting channel was identified by XBIC. Subsequently, a μ-XRF line scan with long acquisition time per point was performed across the current collecting channel location. As shown in Fig. 4, copper and iron were found to be present at the current collecting channel (bounded between the dashed lines). Lower bounds for the peak metal concentrations were determined, accurate within a factor of 2 by comparison with calibration standards, to be 1.7×10^{14} cm^{-2} for Fe and 1.5×10^{14} cm^{-2} for Cu, by assuming the metals lie very near to the wafer surface. If the detected impurities lie below the surface, their real concentrations would be higher than those measured, since an XRF signal decays exponentially with distance inside a silicon matrix with an attenuation length of 36 μm for Fe and 70 μm for Cu.

The width of the iron peak is close to the diameter of the incident x-ray beam, which indicates that iron formed precipitates localized within a diameter equal to or smaller than the beam size. The copper peak is much broader that the iron, indicating that copper more likely forms a colony of small precipitates that appear to decorate an extended defect, which is a well-known property of copper in silicon (see Istratov *et al.*,[31] and references therein). It is also known that copper precipitation is enhanced in n-type silicon by Fermi level effects,[32] which would increase the likelihood of copper precipitation in the layer of inverse conductivity type surrounding the channel. Further evidence for the existence of Fe and Cu in precipitate form is the fact that the metal concentrations measured by μ-XRF are well above the upper limit of their dissolved concentrations at room temperature.

At present, the precise role of metal clusters in the formation and electrical properties of current collecting channels cannot be determined from experimental evidence with absolute certainty; however, a few possibilities should be pointed out. The first possibility is related to an enhanced recombination current in the space charge region surrounding the current collecting channels. Theoretical and experimental results have shown that for pn junctions with donor-like recombination centers, ideality factors greater than 2 can be observed with the saturation of the recombination current for limited bias ranges.[33] However, this interpretation is in contradiction with the excellent collection efficiency of the current collecting channels; if a multitude of recombination centers were present, it is likely that a noticeable fraction of the carriers would recombine before reaching the channels, hereby degrading the current collection efficiency of these channels. Recombination centers in the space charge region surrounding the current collecting channel would not significantly affect the transport of carriers along the channel, just as recombination in the emitter space charge region does not significantly affect the transport of electrons in the emitter.

The more likely possibility is the inversion channel model proposed by Breitenstein *et al.*[26] This model assumes positive fixed charges at the cores of the current collecting channels. Transition metal precipitates could play a role in this model, since it is well-known that such precipitates at structural defects may be charged, thus attracting minority carriers.[34] However, these fixed charges at the cores of current collecting channels would not be recombination-active because they would either be buried beneath insulating oxide precipitates or lying in a wide gap material such as SiC. At

zero bias voltage, these fixed charges attract minority carriers to the current collecting channels, where the minority carriers cannot recombine and thus can diffuse over macroscopic distances. Under forward bias, according to the inversion channel model, the barrier height of the pn junction surrounding these channels is reduced due to the bias-dependent charge balance at the channel / bulk Si interface. This explains why these channels operate predominantly as current collectors at zero bias voltage, and can induce shunting at higher forward biases. Further investigations need to be made to determine the precise role of metals in the formation and electrical properties of these channels, which was beyond the scope of this study.

V. CONCLUSIONS

An experimental procedure is demonstrated to detect transition metals at shunting locations in solar cells, involving lock-in thermography, SR–LBIC, XBIC, and μ-XRF. Transition metals were found to be present in higher than average concentrations at both shunts analyzed in this study. For the cast mc-Si sample, silver and titanium were measured at the shunt location by μ-XRF in the same relative concentrations as in the contact fingers, suggesting a process-induced error occurred during metallization. For RGS, a material-specific loss mechanism has been described associated with channels of inverse conductivity type extending from the emitter into the bulk. These channels exhibit predominantly carrier collection properties at zero bias voltage (as evidenced in LBIC and XBIC measurements), and thus a comparison of at least two LBIC maps with excitation radiation penetration depths smaller and larger than the minority carrier diffusion length allows one to determine the locations of current collecting channels. At higher forward bias voltages, shunting has been revealed by lock-in thermography at the channel locations. These results can be explained most effectively by the presence of fixed charges at the cores of the channels (to which metals, revealed by μ-XRF, may contribute), which cause local band bending in the vicinity of the channel to occur, thus attracting minority charges to the channels. Recombination pathways are blocked by the presence of insulating or wide band gap materials, allowing for the transport of carriers over large distances. At forward bias voltages, the inversion channels represent a potential groove for electrons coming from the emitter, resulting in a locally reduced barrier height and in the presence of a shunting current. Now that it is established that transition metal precipitates are indeed present at current collecting channels, future investigations are required to determine the extent to which these impurities affect the formation and electrical properties of these channels.

ACKNOWLEDGMENTS

The authors would like to thank C. Ballif, S. Peters, S. Glunz, and Do. Huljic of Fraunhofer ISE as well as D. Freeman of UC Berkeley for insightful discussions. A. Thompson and M. Marcus of the Advanced Light Source are recognized for their assistance at the synchrotron. E. Schäfer is thanked for performing SR–LBIC measurements on the cast multicrystalline sample, as is A. Neugebauer for his rigorous review of the manuscript. This research was made possible by NREL Subcontract No. AAT-2-31605-03, AG-Solar project of the government of Northrhein-Westfalia (NRW), funded through the Fraunhofer Institute for Solar Energy Systems (Germany), and the German KOSI Project. The Advanced Light Source is supported by the Director, Office of Science, Office of Basic Energy Sciences, Materials Sciences Division, of the U.S. Department of Energy under Contract No. DE-AC03-76SF00098 at Lawrence Berkeley National Laboratory.

[1] T. F. Ciszek (private communication).
[2] M. A. Green, K. Emery, D. L. King, S. Igari, and W. Warta, Prog. Photovoltaics **11**, 39 (2003).
[3] D. Macdonald, A. Cuevas, A. Kinomura, and Y. Nakano, *Proceedings of the 29th IEEE PVSC*, New Orleans, LA, 2002, p. 285.
[4] A. A. Istratov, T. Buonassisi, R. J. McDonald, A. R. Smith, R. Schindler, J. A. Rand, J.P. Kalejs, and E. R. Weber, J. Appl. Phys. **94**, 6552 (2003).
[5] J. R. Davis, A. Rohatgi, R. H. Hopkins, P. D. Blais, P. Rai-Choudjury, J. R. McCormick, and H. C. Mollenkopf, IEEE Trans. Electron Devices **27**, 677 (1980).
[6] C. H. Chan and C. T. Sah, IEEE Trans. Electron Devices **26**, 937 (1979).
[7] J. Lindmayer, COMSAT Tech. Rev. **2**, 105 (1972).
[8] C. T. Sah, R. N. Noyce, and W. Shockley, Proc. IRE **45**, 1228 (1957).
[9] B. L. Sopori, Mater. Sci. Forum **258–263**, 527 (1997).
[10] J. Carstensen, G. Popkirov, J. Bahr, and H. Föll, Sol. Energy Mater. Sol. Cells **76**, 599 (2003).
[11] C. Ballif, S. Peters, T. Zerres, J. Isenberg, D. Borchert, and G. Willeke, *Proceedings of the 12th Workshop on Crystalline Silicon Solar Cell Materials and Processes*, edited by B. L. Sopori (NREL, Golden, CO, 2002), p. 136.
[12] O. Breitenstein, M. Langenkamp, O. Lang, and A. Schirrmacher, Sol. Energy Mater. Sol. Cells **65**, 55 (2001).
[13] O. Breitenstein and M. Langenkamp, *Proceedings of the 2nd WCPEC*, Vienna, Austria, 1998, p. 1382.
[14] O. Breitenstein, J. P. Rakotoniaina, S. Neve, M. H. Al Rifai, and M. Werner, *Proceedings of the 3rd WCPEC*, Osaka, Japan, 2003.
[15] H. Lange and I. A. Schwirtlich, J. Cryst. Growth **104**, 108 (1990).
[16] O. Breitenstein, M. Langenkamp, F. Altmann, D. Katzer, A. Lindner, and H. Eggers, Rev. Sci. Instrum. **71**, 4155 (2000).
[17] www.thermosensorik.com.
[18] S. A. McHugo *et al.*, J. Appl. Phys. **89**, 4282 (2001).
[19] J. H. Underwood, A. C. Thompson, Y. Wu, R. D. Giauque, K. W. Jones, and M. L. Rivers, Nucl. Instrum. Methods Phys. Res. A **266**, 318 (1988).
[20] S. A. McHugo *et al.*, J. Cryst. Growth **210**, 395 (2000).
[21] S. A. McHugo, A. C. Thompson, I. Périchaud, and S. Martinuzzi, Appl. Phys. Lett. **72**, 3482 (1998).
[22] O. F. Vyvenko, T. Buonassisi, A. A. Istratov, H. Hieslmair, A. C. Thompson, R. Schindler, and E. R. Weber, J. Appl. Phys. **91**, 3614 (2002).
[23] G. Hahn, C. Zechner, M. Spiegel, W. Jooss, P. Fath, G. Willeke, and E. Bucher, *Proceedings of the 2nd WEPEC*, Vienna, 1998, p. 1840.
[24] G. Hahn, D. Sontag, and C. Häßler, Sol. Energy Mater. Sol. Cells **72**, 453 (2002).
[25] C. Häßler, H.-U. Höfs, S. Thurm, O. Breitenstein, and M. Langenkamp, *Proceedings of the 16th EC-PVSEC*, Glasgow, United Kingdom, 2000, p. 1352.
[26] O. Breitenstein, M. Langenkamp, and J. P. Rakotoniaina, Diffus. Defect Data, Pt. B **78–79**, 29 (2001).
[27] H. Gottschalk, Phys. Status Solidi B **222**, 353 (2000).
[28] C. T. Sah, R. N. Noyce, and W. Shockley, Proc. Inst. Radio Engrs. **49**, 603 (1961).
[29] S. C. Choo, Solid-State Electron. **11**, 1069 (1968).
[30] S. C. Choo, Solid-State Electron. **14**, 1201 (1971).
[31] A. A. Istratov and E. R. Weber, J. Electrochem. Soc. **149**, G21 (2002).
[32] C. Flink, H. Feick, S. A. McHugo, W. Seifert, H. Hieslmair, T. Heiser, A. A. Istratov, and E. R. Weber, Phys. Rev. Lett. **85**, 4900 (2000).
[33] J. Beier, and B. Voß, *Proceedings of the 23rd IEEE-PVSC*, Louisville, KY, 1993, p. 321.
[34] V. Kveder, M. Kittler, and W Schröter, Phys. Rev. B **63**, 115208 (2001).